文章编号：1001-9014(2023)05-0652-07

DOI:10.11972/j.issn.1001-9014.2023.05.010

Selenium microrods-based broadband photodetector

YU Xiang-Xiang[1,2], ZHANG Heng[2], WANG Bao-Lin[2], MIAO Xiang-Shui[1,3], YE Lei[1,3*]

(1. School of Integrated Circuits, Huazhong University of Science and Technology, Wuhan 430074, China;
2. School of Physic and Optoelectronic Engineering, Yangtze University, Jingzhou 434023, China;
3. Hubei Yangtze Memory Laboratories, Wuhan 430205, China)

Abstract: In this paper, Se microrods were synthesized using a physical vapor deposition method, and a metal-semiconductor-metal (MSM) photodetector was fabricated by using silver paste as the electrode. This photodetector exhibits a fast response time (T_r = 41 ms, T_d = 46 ms), excellent responsivity (18.32 mA/W), and detectivity (1.65×10^8 Jones) at 3 V bias and under 450 nm light illumination. Spectral measurements demonstrate that the device has a broadband detection range from visible to near infrared range (450~1 550 nm). Additionally, the device can also perform self-powered detection without bias. This research will further improve the application and development of Se in broadband photodetection.

Key words: photodetector, broadband photodetection, self-powered detection, Se microrod

基于硒微米棒的宽光谱响应的光电探测器

余翔翔[1,2], 张 恒[2], 王宝霖[2], 缪向水[1,3], 叶 镭[1,3*]

(1. 华中科技大学集成电路学院,湖北 武汉 430074;
2. 长江大学物理与光电工程学院,湖北 荆州 434023;
3. 湖北省江城实验室,湖北 武汉 430205)

摘要:采用物理气相沉积法合成硒微米棒,并以银浆为电极制备了金属-半导体-金属结构的光电探测器。该光电探测器在3 V偏压和450 nm光照下具有快速的响应速度(上升时间=41 ms,下降时间=46 ms),优异的响应度(18.32 mA/W)和探测率(1.65×10^8 Jones)。光谱测试表明器件具有从可见光到近红外的宽光谱探测能力(450~1 550 nm)。此外,该器件还可以在无偏压下进行自供能探测。本研究将进一步完善硒半导体在宽光谱光电探测中的应用和发展。

关 键 词:光电探测器;宽光谱探测;自供能探测;硒微米棒

中图分类号:O43; **文献标识码**:A

Introduction

Nowadays, semiconductors are widely used in energy storage, environmental sensing, neuromorphic systems, *etc*[1-3]. Among these applications, photodetectors with the ability to convert optical signal into electrical signal, play an important role in sensing network system including imaging, night vision, optical communication and security inspection[4-7]. At present, the most widely used is silicon-based commercial photodetector, which exhibits fast response speed, high responsivity and large signal-to-noise ratio. However, its high intrinsic band gap (1.12 eV) limits the detection range to below 1100 nm. To fulfill the needs of infrared imaging and other fields, it is urgent to develop high performance broadband infrared photodetectors. To date, most of the commercial infrared photodetectors are based on traditional materials such as InGaAs, InSb, HgCdTe[8-11]. However, the expensive material growth procedure and the dependence on refrigeration equipment to reduce dark current restrict their further application. Therefore, it is necessary to develop an infrared detector that is easy to use, inexpensive, and of good performance.

As a typical P-type semiconductor, Se (Selenium)

Received date: 2023-03-07, **revised date**: 2023-06-07 **收稿日期**:2023-03-07,**修回日期**:2023-06-07

Foundation items: Supported by the National Natural Science Foundation of China (11304092, 51371079, 11305056, 11304299, 51602099).

Biography: Yu Xiang-Xiang (1990-), doctor, Wuhan. Research area involves Semiconductor materials and devices. E-mail: yuxx518@126.com.

* **Corresponding author**: E-mail: leiye@hust.edu.cn

exhibits many excellent optoelectronic properties, such as fast response speed and large photoconductivity. The first photoconductor based on Se was reported by Smith in 1873[12]. After that, virous Se-based photodetectors have been designed. Karim *et al*. used amorphous Se to convert and detect the X-rays[13]. Pan *et al*. systematically studied the effects of hole-blocking dielectric layer on the microstructure and visible photoconductive properties of polycrystalline Se thin films[14]. In addition to thin films, various nanostructures have also been synthesized. Due to the chain-like molecular structure, Se spontaneously delivers 1D morphologies. Fang *et al*. fabricated a plasmonic enhanced *t*-Se microtube photodetector[15]. Wang *et al*. constructed a Se nanobelt-based transistor, where the hole mobility and concentration were estimated to 0.63 $cm^2 (V\ s)^{-1}$ and 9.35×10^{16} cm^{-3} respectively[16]. These studies have promoted the application of Se in photodetection. However, the intrinsic wide bandgap of Se (1.77 eV) limits its application in the infrared range. To further improve the detection range of the device, a common approach is to construct heterojunctions with other infrared materials[17, 18]. In addition, using defect absorption to improve the detection range is also an effective method. For example, blocked impurity band (BIB) infrared detectors employ a layer of material doped with specific impurities to create defect states within the bandgap, which can absorb specific wavelengths of infrared radiation. The absorbed radiation generates electron-hole pairs, which are collected by an electric field and converted into an electrical signal, enabling the detection of various wavelengths of infrared radiation[19]. However, BIB detectors rely on complex doping processes. In contrast, employing defects that spontaneously generated during material growth to achieve infrared absorption is a simpler approach. In our previous work, a broadband photodetection up to 1550 nm has been obtained based on Se self-supporting polycrystalline film, which demonstrates the potential of selenium in infrared detection[20]. However, since the thin film has an amorphous structure, the recombination of carriers at the grain boundary significantly reduces the responsivity of the device.

In this work, we employed a low-temperature and catalyst-free method to prepare one-dimensional Se microrods with a single crystal structure, which is advantageous for efficient carrier transport. After constructing electrodes at each end of the microrod with conductive silver paste, a MSM (metal-semiconductor-metal) type photodetector has been fabricated. During the photodetection test, the device exhibits broadband detection spectrum (450 ~ 1550 nm), fast response speed (T_r = 41 ms, T_d = 46 ms), large responsivity (18.32 mA/W) and detectivity (1.65×10^8 Jones). Besides, it can also exhibit self-powered photodetection capability under zero bias due to the different Schottky barrier height between the two ends of the microrod and the electrode. These results fully demonstrate the application of Se in broadband photodetection.

1 Experiments

Materials growth and characterization: Se microrods were prepared using the physical vapor deposition (PVD) method. Fig. 1(a) illustrates the schematic diagram of the synthesis process. Firstly, high-purity Se powder was placed in the quartz boat. Subsequently, the quartz boat was pushed to the heating center of the horizontal tube furnace, and a piece of clean glass was placed down steam. To remove air, the tube was pumped and flushed with Argon and repeated three times. During the growth, the tube furnace was heated to 250℃ in 50 min and held for 2 hours with 100 sccm Argon flow. Following the growth period, the furnace was allowed to cool naturally to room temperature. As a result, bright black Se products were obtained on the glass substrates.

The crystal structure was characterized by the powder X-ray diffraction (Empyrean, PANalytical Company), and the scanning range 2θ is 10°~90°. The morphology was obtained by the Scanning Electron Microscope (MIRA3, Czech Tesken Company). The optical absorption spectrum was measured by UV-Vis-NIR spectroscopy (SolidSpec-3700, SHIMADZU Company). The Raman spectrum was collected on a Raman spectrometer with an excitation wavelength of 532 nm (LabRAM HR800, Horiba JobinYvon Company).

Device fabrication: With the help of the surface tension of water, a single Se microrod with smooth surface and uniform diameter can be attached to the metal needle through a drop of water and transferred onto the glass substrate. After that, the conductive silver paste was uniformly coated on both ends of the microrod. Finally, the device was annealed at 110℃ in high-purity Argon atmosphere to improve interface contact quality. The schematic diagram and optical image of the device are shown in Fig. 1(b) and Fig. 1(c).

Device Performance Characterization: The photoresponse was measured by the Semiconductor analyzer (Keithley 4200A-SCS) system and monochromatic light source. The light source is a series of single-mode fiber-pigtailed lasers of different wavelengths, which illumination intensity and light on-off frequency can be controlled by the current and temperature controller (ITC4001).

2 Results and discussions

Fig. 2 (a) shows the scanning electron microscope (SEM) image of a Se microrod on conductive carbon tape. The diameter of the microrod is about 35 μm and the surface is smooth, indicating that the Se microrods are suitable for making photodetectors by hand. To verify the crystal structure of the product, X-ray diffraction was collected, and the corresponding pattern is shown in Fig. 2 (b). All diffraction peaks can correspond to the standard pattern of Se (PDF#06-0362), which indicates the high purity of our products. From the pattern results, the synthesized microrods exhibit a triangular structure, and the lattice constants are $a = b = 4.366$ Å, $c = 4.954$ Å.

The optical absorption spectrum of as prepared Se

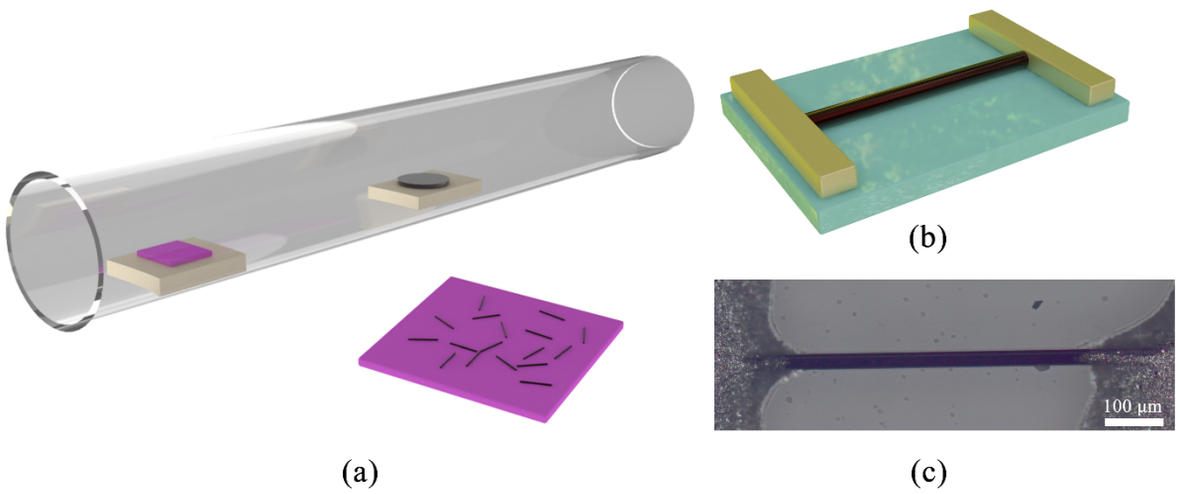

Fig 1 (a) The schematic diagram of the synthesis process, (b) the schematic diagram of the device, (c) the optical image of the device.
图 1 (a) 材料制备示意图, (b) 器件模型图, (c) 器件实物图。

microrods within 350 - 1800 nm is shown in Fig. 2 (c). The light absorption of Se products was higher in the wavelength range of 350 ~ 680 nm but decreased significantly when the wavelength larger than 680 nm. From the illustration in Fig. 2 (c), the band gap of Se microrods is about 1.71e V, which is consistent with the bulk Se. From the Raman spectrum in Fig. 2 (d), their two strong Raman peak located at 144 cm^{-1} and 237 cm^{-1}. The Raman resonance peak at 237 cm^{-1} is the A_1 mode, which is the characteristic stretching mode of the chain-like structure and only exists in triangular selenium. The other peak located at 144 cm^{-1} is the E_1 mode, corresponding to the transverse optical phonon mode. This Raman result is consistent with the XRD pattern in Fig. 2 (b), indicating the synthesized Se microrods belong to triangular selenium.

To study the photoelectric properties of the selenium microrod. A series of photoelectric tests were carried out. Fig. 3 (a) shows the current voltage (*I-V*) curves of the Se microrod photodetector in dark and under 450 nm light illumination. It is clear that the current increases significantly after illumination. As the light intensity is increased, the current also increases synchronously. However, when the intensity is increased to 2.958 mW/mm^2, the photocurrent tends to saturate. In the case of the Se microrod photodetector, it works based on the principle of photoconductivity. When it is illuminated by light, the absorbed photons create electron-hole pairs. The generated electrons and holes can then be separated by the built-in electric field within the material and contribute to the electrical current that flows through the device. As the light intensity increases, more photons are absorbed, and more electron-hole pairs are generated, leading to an increase in the electrical current. However, when the light intensity reaches a certain level, the number of electron-hole pairs becomes saturated, and the photocurrent no longer increases. Besides, when rising the bias voltage, the photocurrent also increases, which shows a synergistic effect between light and potential. Fig. 3 (b) shows the transient response behavior of the photodetector under 450 nm light intensity of 3.845 mW/mm^2 at a 3 V bias voltage, which shows the device exhibits a fast and stable switching characteristic. The response speed is also an important performance parameter. By intercepting part of the *I-T* curve, the rise and decay time in Fig. 3 (c) are calculated to be 41 and 46 ms. In addition to the above parameters, the responsivity (R) and detectivity (D^*) are also two important indicators to evaluate the photo detecting performance. Where R is the efficiency of the photodetector in converting the optical signal into electrical signal, and D^* is the detect potential of weak light signals. These two important parameters can be derived using the following equations [21-23].

$$R = \frac{I_{ph} - I_d}{PS} \quad ,(1)$$

$$D^* = \frac{RS^{1/2}}{(2eI_d)^{1/2}} \quad ,(2)$$

where I_{ph} is the photocurrent, I_d is the dark current, P is the optical power density of the incident light source, S is the effective area of the detector irradiated by light, and e is the basic charge. To quantify the two key parameters, the responsivity and detectivity curves of the detector under 3 V and -3 V bias voltages and different light intensities are plotted in Fig. 3 (d). The results show that the responsivity and detectivity of the selenium microrod photodetector at the same bias voltage decrease with the increment of light intensity. This is because when the light intensity is too high, the number of photons absorbed by the photodetector exceeds the number of available carriers, leading to carrier saturation. This causes the excess photons to be wasted as heat instead of contributing to the photocurrent, resulting in a decrease in responsivity and detectivity. Under 3 V bias voltage, the maximum $R$and $D^*$are calculated to be 18.32 mA/W and 1.65×10^8 Jones. At the reverse bias

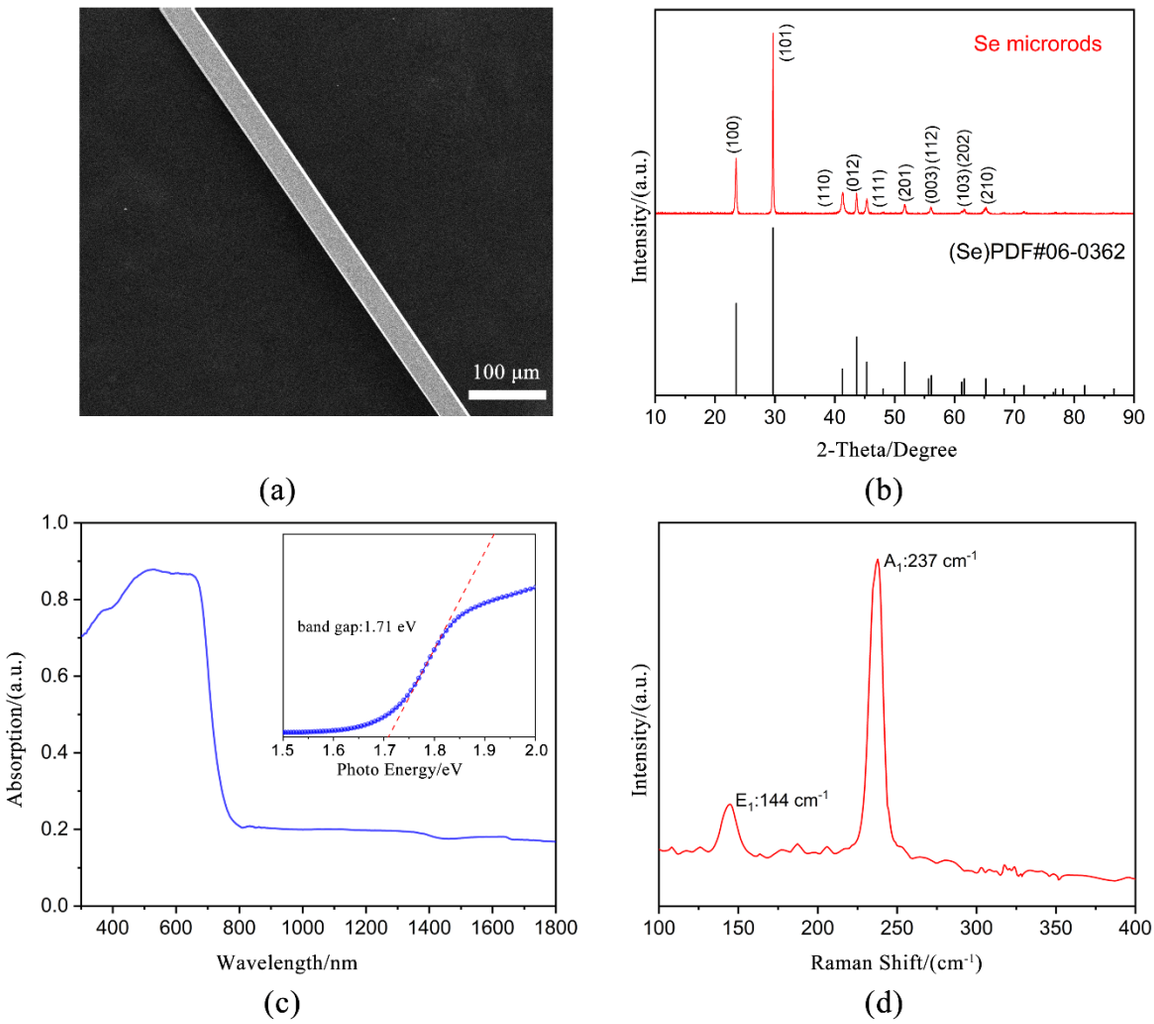

Fig 2　(a) The SEM image of a single Se microrod, (b) the XRD pattern of Se microrods, (c) the absorption spectrum of Se microrods. The insert is the calculated bandgap image, (d) the Raman spectrum of the Se microrod.
图 2　(a) 硒微米线扫描电镜图, (b) 硒微米线 XRD 图谱, (c) 硒微米线吸收图谱. 插图为硒微米线禁带宽度图, (d) 硒微米线拉曼图谱。

voltage of -3 V, the calculated results are 21.33 mA/W and 1.91×10^{8} Jones. The above differences can be explained by the *I-V* curves in Fig. 3 (a). The asymmetric curves show the presence of the Schottky barrier between the material and the electrode. As the work function of the pure Ag metal is about 4.6 eV, it tends to form ohmic contact with Se. But for the silver paste, it is a complex mixture and difficult to maintain a fixed work function. Kinds of literatures have reported that silver paste can form both ohmic contact and Schottky contact with the same semiconductor material[24, 25]. For our device, the difference in barrier height and contact area leads to different built-in potential at both ends of the electrode, which leads to the above different results.

To investigate the broadband detection potential, we test the photocurrent under laser illumination with different wavelengths from 785 to 1550 nm. It can be seen from Fig. 4 (a) that the device has good detection performance for all the five selected light sources, and these results promote the detection potential of Se to the infrared range. Fig. 4 (b) shows the *R*and $D^{*}$of the device under each light illumination. Compared with the test results under 450 nm illumination, the above results are much smaller. Since the above wavelengths exceed the intrinsic absorption cutoff wavelength of selenium, the above photogenerated carriers can be attributed to defect absorption. For the Se nanostructures synthesized by thermal evaporation, it usually forms an amorphous layer on the surface. The amorphous layer is easily to be terminated by H-, O-, OH-, thus forming surface defects[12, 16, 20]. As the defect energy level is only about 0.4 to 1.0 eV, the absorption range can be greatly improved. However, the low absorption efficiency of the defects leads to lower performance indicators for photodetection.

To further expand the application range of devices, we tested the self-powered detection capability of the device. Although the device is a photoconductor, the different barrier height enables it to have the potential of self-powered detection. Fig. 4 (c) exhibits the *I-T* curve of the device under 450 nm illumination without bias volt-

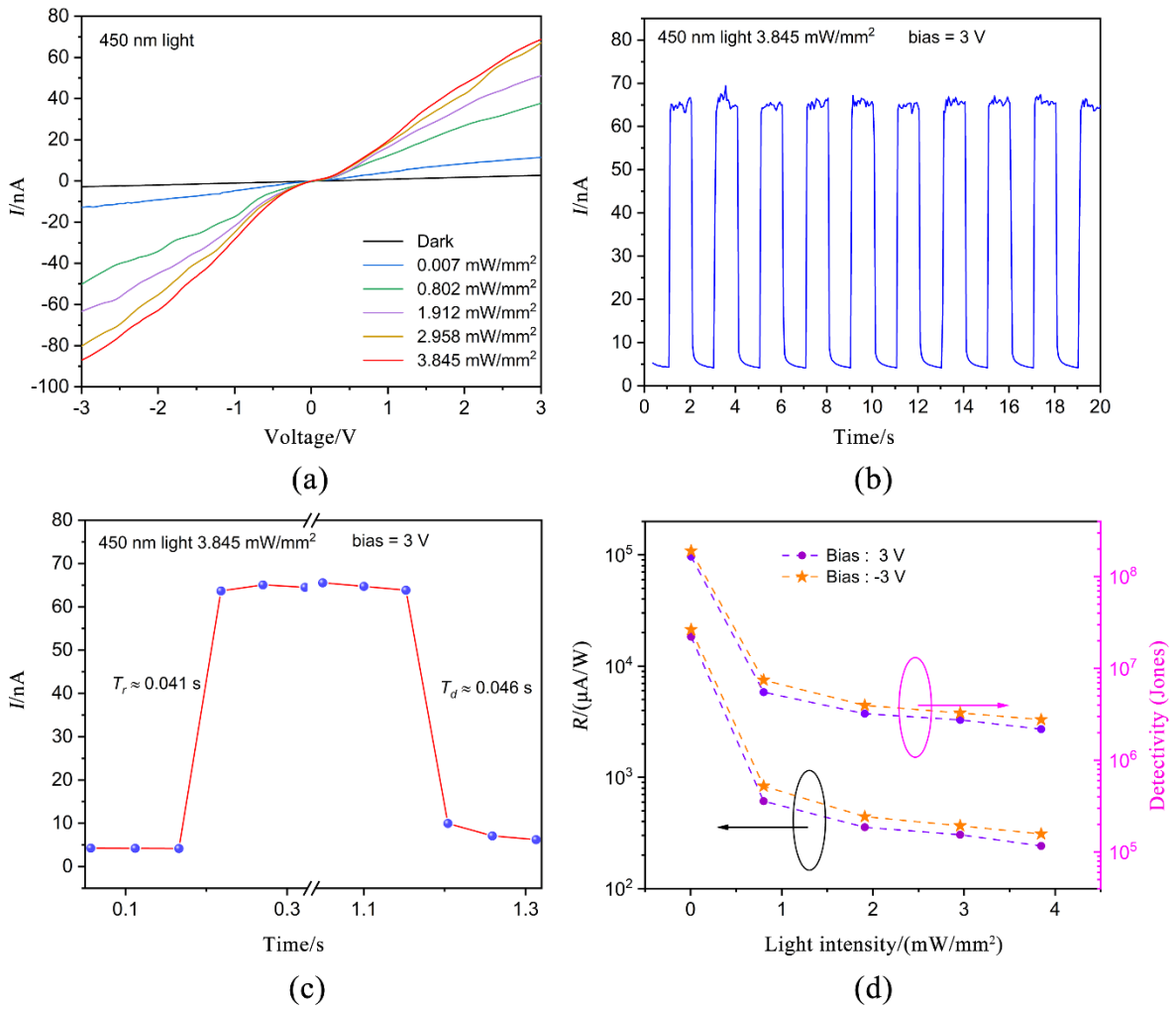

Fig. 3 (a) The *I-V* curves of the device in dark and under 450 nm illumination with different light intensities, (b) the *I-T* curve of the devices under 450 nm illumination at 3 V bias voltage, (c) the response time of the device under 450 nm illumination at 3 V bias voltage, (d) The responsivity and detectivity of the device under 450 nm illumination with different light intensities at ±3 V bias voltage。

图 3 (a) 暗态和450 nm光照下器件电流-时间图, (b) 450 nm光照和3 V偏压下时间-电流图, (c) 450 nm光照和3 V偏压下响应时间图, (d) 450 nm不同强度光照和±3 V偏压下器件响应度和探测率图。

age, a fast and stable switching characteristic can also be obtained. Further response speed analysis in Fig. 4 (d) shows that the rise time and decay time of the device is 8 ms and 12 ms, respectively.

As shown in table 1, we present a comparison of the optoelectronic performance indicators of our device with those of other photodetectors based on selenium materials. Although our device's performance metrics are not as impressive as those reported in the literature, it does exhibit a wide spectral response. Interestingly, when compared to other devices with a similar spectral response, our device's metrics appear to have certain advantages. Further research could be conducted to optimize the performance of our device and to investigate the underlying mechanisms that give rise to its unique characteristics.

Table 1 Performance indicators comparison of this work with other typical photodetectors based on Se materials
表1 本工作与其他典型硒基光电探测器性能指标对比

Devices	R [mA/W]	D^* [Jones]	Time [ms]	Wavelength [nm]	Detection range [nm]	Ref.
Se microtube	19		0. 32/23. 02	610	350~700	[15]
Se nanobelt	3.27×10^{7}		0. 57/2. 65	600	300~750	[16]
Se microrod	294	9.4×10^{12}	0. 12/0. 15	365	300~800	[26]
Se 1D/2D structure	6		25/25	638	405~1555	[12]
Se film	8.1×10^{-3}	1.3×10^{5}	4. 5/63. 8	450	450~1550	[20]
Se microrod	18. 32	1.65×10^{8}	41/46	450	450~1550	This Work

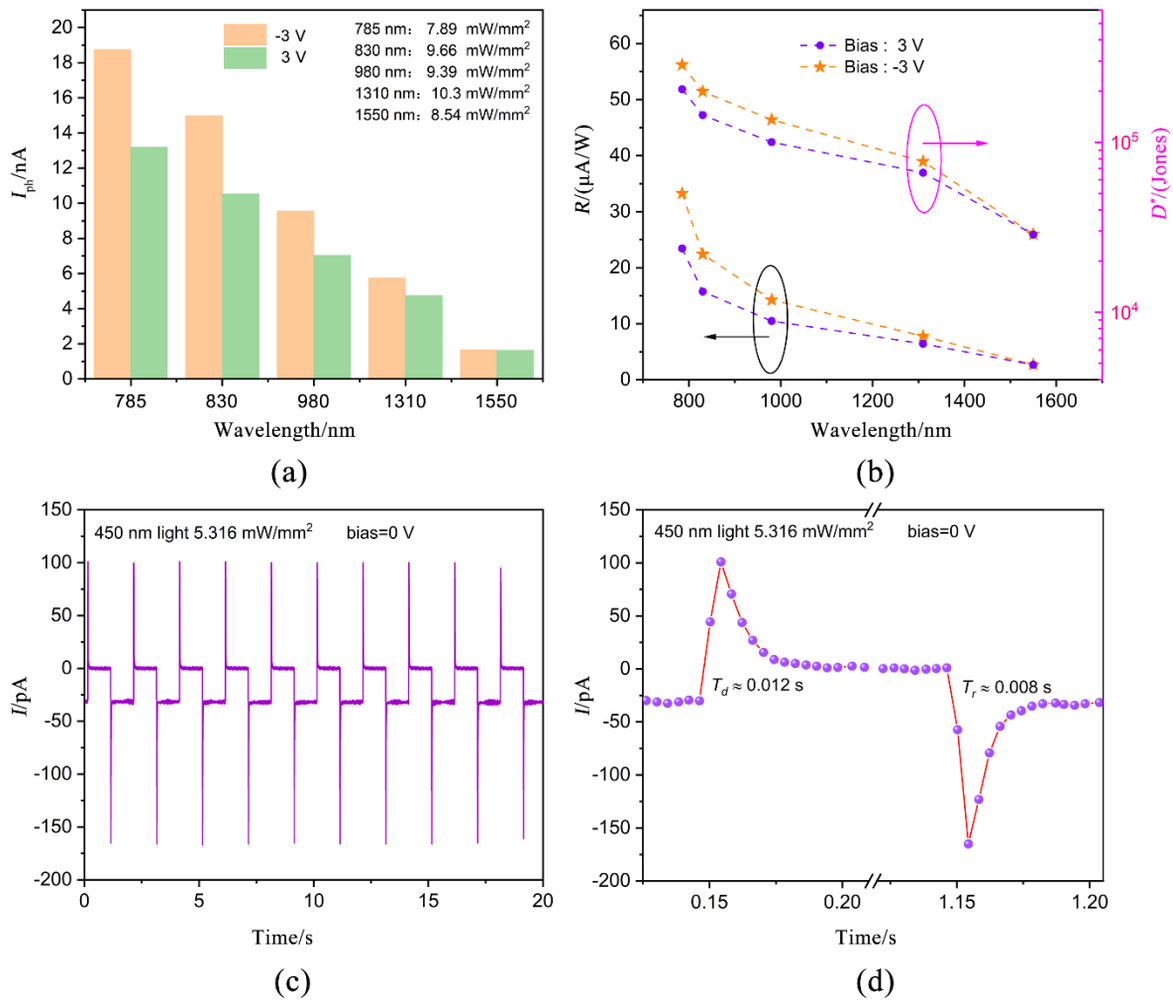

Fig. 4　(a) The photocurrent distribution of the device under light illumination with different wavelengths, (b) the responsivity and detectivity of the device under light illumination with different wavelengths at ±3 V bias voltage, (c) the I-T curve of the device under 450 nm illumination without bias, (d) the response time of the device under 450 nm illumination without bias.
图 4　(a) 不同波长光照和±3 V偏压下光电流图, (b) 不同波长光照和±3 V偏压下响应度和探测率图, (c) 450 nm光照和0 V偏压下电流-时间图, (d) 450 nm光照和0 V偏压下器件响应时间图。

3　Conclusions

In conclusion, we have fabricated a MSM photodetector based on Se microrods with a simple materials growth method and low-cost device fabrication process. Compared with traditional Se based photodetectors, the device has a broadband photodetection from visible to infrared range. In addition, due to the difference of Schottky barrier at both ends of the electrode, the device can also perform self-powered photodetection without bias. The research results of this paper not only improve the application of Se in infrared detection field, but also expand the application flexibility of device.

References

[1] Yin H, Han D Y, Yu X X, *et al*. Recent Advances in Electrospun Metal Chalcogenide Anodes for Lithium-Ion and Sodium-Ion Batteries [J]. *ACS Applied Energy Materials*, 2023, **6** (3): 1155-1175.
[2] Wang P, Xia H, Li Q, *et al*. Sensing Infrared Photons at Room Temperature: From Bulk Materials to Atomic Layers [J]. *Small*, 2019, **15** (46): 1904396.
[3] Tong L, Peng Z, Lin R, *et al*. 2D materials based homogeneous transistor-memory architecture for neuromorphic hardware [J]. *Science*, 2021, **373** (6561): 1353-1358.
[4] Li C, Wang H, Wang F, *et al*. Ultrafast and broadband photodetectors based on a perovskite/organic bulk heterojunction for large-dynamic-range imaging [J]. *Light: Science & Applications*, 2020, **9** (1): 31.
[5] Kumar M, Lim S, Kim J, *et al*. Picoampere Dark Current and Electro-opto-coupled Sub-to-Super-linear response from Mott-transition enabled Infrared Photodetector for Near-sensor Vision processing [J]. *Advanced Materials*, 2023: 2210907.
[6] Li L, Wang D, Zhang D, *et al*. Near-Infrared Light Triggered Self-Powered Mechano-Optical Communication System using Wearable Photodetector Textile [J]. *Advanced Functional Materials*, 2021, **31** (37): 2104782.
[7] Chen Y, Ma W, Tan C, *et al*. Broadband Bi_2O_2Se Photodetectors from Infrared to Terahertz [J]. *Advanced Functional Materials*, 2021, **31** (14): 2009554.
[8] Peng M, Xie R, Wang Z, *et al*. Blackbody-sensitive room-temperature infrared photodetectors based on low-dimensional tellurium grown by chemical vapor deposition [J]. *Science Advances*, 2021, **7** (16): eabf7358.
[9] Hu W D, Chen X S, Ye Z H, *et al*. A hybrid surface passivation on HgCdTe long wave infrared detector with in-situ CdTe deposition and high-density hydrogen plasma modification [J]. *Applied Physics*

Letters, 2011, **99**(9): 091101.
[10] Guo J X, Xie R Z, Wang P, *et al*. Infrared photodetectors for multi-dimensional optical information acquisition [J]. *Journal of Infrared and Millimeter Waves*, 2022, **41**(1): 40-60.
[11] Hu W D, Ye Z H, Liao L, *et al*. 128× 128 long-wavelength/mid-wavelength two-color HgCdTe infrared focal plane array detector with ultralow spectral cross talk [J]. *Optics Letters*, 2014, **39**(17): 5184-5187.
[12] Chen Y Z, You Y T, Chen P J, *et al*. Environmentally and Mechanically Stable Selenium 1D/2D Hybrid Structures for Broad-Range Photoresponse from Ultraviolet to Infrared Wavelengths [J]. *ACS Applied Materials & Interfaces*, 2018, **10**(41): 35477-35486.
[13] Abbaszadeh S, Allec N, Wang K, *et al*. Low Dark-Current Lateral Amorphous-Selenium Metal - Semiconductor - Metal Photodetector [J]. *IEEE Electron Device Letters*, 2011, **32**(9): 1263-1265.
[14] Chang C Y, Pan F M, Lin J S, *et al*. Lateral amorphous selenium metal-insulator-semiconductor-insulator-metal photodetectors using ultrathin dielectric blocking layers for dark current suppression [J]. *Journal of Applied Physics*, 2016, **120**(23): 234501.
[15] Hu K, Chen H Y, Jiang M M, *et al*. Broadband Photoresponse Enhancement of a High-Performance t-Se Microtube Photodetector by Plasmonic Metallic Nanoparticles [J]. *Advanced Functional Materials*, 2016, **26**(36): 6641-6648.
[16] Luo L B, Yang X B, Liang F B, *et al*. Transparent and flexible selenium nanobelt-based visible light photodetector [J]. *CrystEngComm*, 2012, **14**(6): 1942-1947.
[17] Yang W, Hu K, Teng F, *et al*. High-Performance Silicon-Compatible Large-Area UV-to-Visible Broadband Photodetector Based on Integrated Lattice-Matched Type II Se/n-Si Heterojunctions [J]. *Nano Letters*, 2018, **18**(8): 4697-4703.
[18] Zhang Y, Zhang F, Xu Y G, *et al*. Epitaxial Growth of Topological Insulators on Semiconductors (Bi_2Se_3/Te@Se) toward High-Performance Photodetectors [J]. *Small Methods*, 2019, **3**(12): 1900349.
[19] Xiao Y L, Zhu H, Deng K, *et al*. Progress and challenges in blocked impurity band infrared detectors for space-based astronomy [J]. *Science China Physics, Mechanics & Astronomy*, 2022, **65**(8): 287301.
[20] Zhang H, li L, Zheng D S, *et al*. Broadband photodetector based on vapor-deposited selenium self-supporting films [J]. *Ceramics International*, 2022, **48**(19): 27750-27757.
[21] Lv T, Huang X Y, Zhang W G, *et al*. High-Responsivity Multiband and Polarization-Sensitive Photodetector Based on the TiS_3/MoS_2 Heterojunction [J]. *ACS Applied Materials & Interfaces*, 2022, **14**(43): 48812-48820.
[22] Tong L, Huang X Y, Wang P, *et al*. Stable mid-infrared polarization imaging based on quasi-2D tellurium at room temperature [J]. *Nature Communications*, 2020, **11**(1): 2308.
[23] Wu S Q, Chen Y, Wang X D, *et al*. Ultra-sensitive polarization-resolved black phosphorus homojunction photodetector defined by ferroelectric domains [J]. *Nature Communications*, 2022, **13**(1): 3198.
[24] Zhou J, Fei P, Gu Y D, *et al*. Piezoelectric-Potential-Controlled Polarity-Reversible Schottky Diodes and Switches of ZnO Wires [J]. *Nano Letters*, 2008, **8**(11): 3973-3977.
[25] Kou J Z, Zhang Y, Liu Y D, *et al*. Nano-force sensor based on a single tellurium microwire [J]. *Semiconductor Science and Technology*, 2017, **32**(7): 074001.
[26] Chang Y, Chen L, Wang J Y, *et al*. Self-Powered Broadband Schottky Junction Photodetector Based on a Single Selenium Microrod [J]. *The Journal of Physical Chemistry C*, 2019, **123**(34): 21244-21251.